Simulations of CO2 storage in aquifer models with top surface morphology and transition zones

Shariatipour, SM, Pickup, GE & MacKay, EJ

Original citation & hyperlink:
Shariatipour, SM, Pickup, GE & MacKay, EJ 2016, 'Simulations of CO2 storage in aquifer models with top surface morphology and transition zones' International Journal of Greenhouse Gas Control, vol 54, no. 1, pp. 117-128. DOI: 10.1016/j.ijggc.2016.06.016
https://dx.doi.org/10.1016/j.ijggc.2016.06.016

DOI 10.1016/j.ijggc.2016.06.016
ISSN 1750-5836

Publisher: Elsevier

Corresponding Author: Dr. Seyed Mohammad Shariatipour

Corresponding Author's Email: Seyed.Shariatipour@Coventry.Ac.Uk

Order of Authors: Seyed Mohammad Shariatipour[a*], Ph.D; Gillian E Pickup[b], PhD; [2]Eric J Mackay[b], PhD

[a*] Flow Measurement and Fluid Mechanics Research Centre, Coventry University, Priory Street, Coventry CV1 5FB, UK

[b] Heriot-Watt University, Riccarton, Edinburgh EH14 4AS, UK

Title: Simulations of CO_2 storage in aquifer models with top surface morphology and transition zones

Abstract

When investigating the storage of CO_2 in deep saline formations, many studies assume a smooth, abrupt interface between the storage and the sealing formations. Typically, though, the surface is irregular, due to sedimentological and stratigraphic effects or structural deformation. In this study, the area where the CO_2 migrates beneath the caprock is investigated. A set of numerical simulations were conducted to investigate the impacts of various factors on CO_2 storage, such as top morphology, tilt, k_v/k_h ratio and the presence of a transition zone, where there is a gradational change from storage formation to caprock.

In the models tested, the k_v/k_h ratio was most important during the injection period, but after injection ceased, the tilt was more important. The amplitude of the ridges, which were used to represent the top morphology, did not have a large effect but, as expected hindered or encouraged migration depending on whether they were perpendicular or parallel to the tilt. A transition zone can increase the security of storage by lessening the amount of CO_2 accumulating underneath the caprock. Therefore it is important to characterise the interface in terms of the size of irregularities and also in terms of the existence of any transition zone. The latter has not been addressed in previous works. A simple formula was derived to predict the limiting tilt for trapping to occur in models with a sinusoidal interface with wavelength, λ, and amplitude, A. Although this is a simplified approach, it provides a means of assessing whether the topography of the top surface will give rise to significant trapping or not.

Keywords: CO_2 Storage in Aquifers; Top Surface Morphology; Transition Zones

1. Introduction

Carbon Capture and Storage (CCS) is a possible option to mitigate the rise in anthropogenic CO_2. When CO_2 is injected into a storage formation, it migrates upwards under buoyancy until it reaches the caprock. Some CO_2 will dissolve and some will be trapped at the pore scale (residual trapping) and also some could be trapped in minerals (although not considered here). However most of the CO_2 will remain as a free phase and, if not trapped under an anticline (dome), will migrate laterally at the top of

the storage formation. It is well known from the Sleipner project that CO_2 migration does not occur uniformly in all directions (Jenkins et al. 2015; Zhu et al. 2015; Cavanagh and Haszeldine 2014; Chadwick and Noy, 2010; Cavanagh 2013), due to irregularities in the top surface of the aquifer (See, for example, Chadwick et al. 2009). Bandilla et al. (2014) investigated the effect of model complexity on CO_2 plume modelling at Sleipner using methods ranging from full 3D simulation to a vertical equilibrium assumption. They suggested that the reason some simulation models cannot predict the actual plume footprint is due to the inaccuracy in some parameters in the site model such as top morphology of the caprock. In fact, the identification of the storage complex boundary is one of the critical issues in the application for a CO_2 storage permit (Pearce et al. 2013). Obviously, adequate site characterisation is crucial, but also careful modelling and simulation is required to be able to predict CO_2 migration pathways, and estimate the migration limit.

There are a number of different ways of simulating CO_2 migration in an aquifer, depending on the level of detail required, and the time available for simulation. Some analytical models have been developed which allow the effect of a range of parameters to be assessed rapidly (e.g. Nordbotten et al. 2005; Hesse 2008; MacMinn et al. 2010). Such calculations usually assume simplified physics (i.e. sharp interface between CO_2 and brine, and no dissolution), and a homogeneous model with an abrupt boundary between the aquifer and caprock. At the other extreme, full numerical simulations may be carried out using conventional reservoir simulation, which takes account of processes such as dissolution of CO_2 in brine, and is often used to study the effect of heterogeneities within an aquifer (e.g. Williams et al. 2013; Cavanagh and Haszeldine 2014; Bandilla et al. 2014). A third option is to combine numerical and analytical calculations. For example, Gasda et al. (2009) assumes vertical equilibrium between the CO_2 and formation brine. The equations are solved numerically, but an analytical model is used within a grid block containing a well. This method is useful for assessing sensitivities in a structurally complex formation (i.e. with a varying top surface), such as the Sleipner model (Gasda et al. 2012). However, some simplifications are made, such as ignoring dissolution of CO_2 in brine. Another approach to assessing the effect of irregularities in the aquifer/caprock interfaces was taken by Nilsen et al. (2012). They used a semi-analytical spill-point analysis and vertical equilibrium, and demonstrated that the morphology of the interface has a significant effect on the storage capacity and the migration of CO_2. Goater et al. (2013) studied the effect of top-surface morphology and heterogeneity on the storage capacity in open aquifers. They concluded that the effect of top-surface topography on the storage efficiency could be neglected in models with a very low permeability and a very low aquifer dip angle.

In the present work, we used conventional simulation (ECLIPSE 300 using the CO2STORE option: Schlumberger, 2013) to study the top-surface morphology, so that we can include dissolution of CO_2 in brine. In the CO2STORE module, the mutual dissolution is modelled using the method of Spycher and Pruess (2005). The fugacity of water is calculated using Henry's Law and the fugacity of CO_2 is calculated using the Redlich-Kwong equation of state. In addition, we have simulated other relevant effects, such as tilt and k_v/k_h ratio (ratio of vertical (z) to horizontal (x) permeability). We also

introduce a transition zone, which is a gradational change from sandstone to mudstone just beneath the caprock (Shariatipour et al. 2012). One set of models was created to study the impact of aquifer/caprock morphology, with ridges which were either perpendicular to the tilt ("*perp*" models) or parallel to the tilt ("*para*" models). The second set was created to study the impact of a transition zone (referred to as "*trans*" models). Interbedded shale layers were used in the transition zone.

2. Model Specification

Equation 1 was used to generate top surfaces for the ridges. A simple model was chosen, so that the properties could be studied methodically.

$$Z = Z_0 + A(Sin(\frac{2\pi x}{\lambda})) + x(\tan\theta) \quad (1)$$

where, A refers to the amplitude of the ridges (m), x denotes distance from the injection point in the X (horizontal) direction (m), λ refers to the wavelength, which is 1000 m here, and θ refers to the tilt angle. As depicted in Figure 1, the sizes of all the models are 8 km × 8 km × 100 m. One injector was placed on the left hand side of model and CO_2 was injected through perforations at the bottom of the aquifer (bottom 50 layers). The models represented part of a larger aquifer, and the pore volume of the outer column of cells on the opposite side of where the injector was placed, was multiplied by a factor of 1E+04, to take account of this.

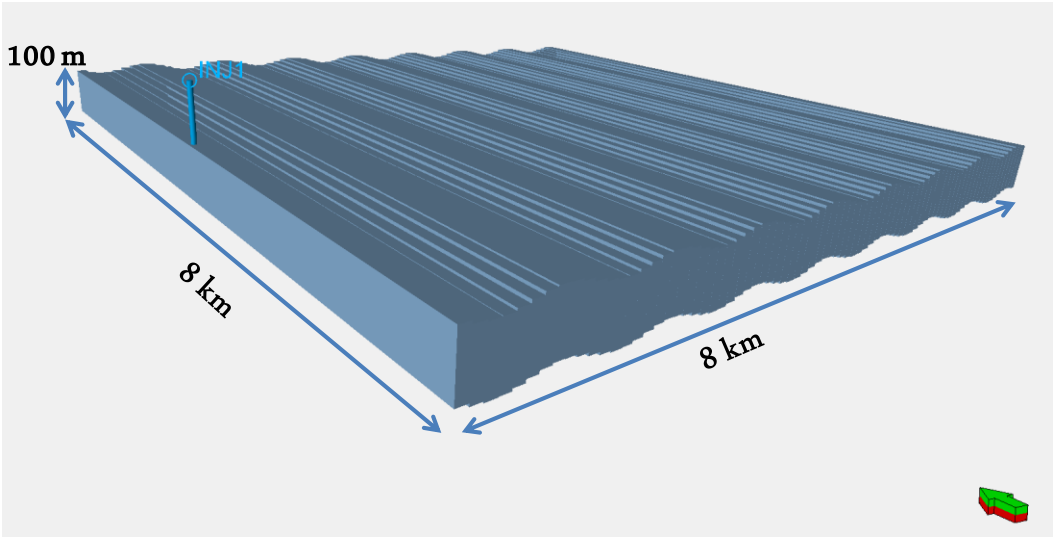

Figure 1 Schematic view of model (vertical exaggeration of 5). The injector was placed at the edge of model on the left side.

Table 1 shows all the scenarios (144 models) that were used in this study. Shariatipour et al. (2016) investigated the effect of different gridding techniques (tilted grid and regular flat Cartesian grid) on CO_2 migration and CO_2 dissolution in saline aquifers. They concluded that the results of CO_2 storage in saline aquifers (distance migrated and the amount of dissolution) are sensitive to the model discretisation. For example using a tilted grid for tilted layers in the storage formation leads to a

decrease in the distance migrated by the CO_2. All the models deployed in this study used a regular flat Cartesian grid to simulate the vertical and lateral migration. All models have the same dimensions and the same grid cell sizes (100 m × 100 m × 1 m), and all were assumed to contain a homogeneous sandstone with porosity of 0.2 and permeability of 500 mD. In the *trans* models, the shales were assume to be impermeable. The same relative permeability curves and capillary pressure were used in all models (Figure 2). These were measured at Heriot-Watt University on a Sherwood sandstone sample as part of the CASSEM project (Smith et al, 2011).

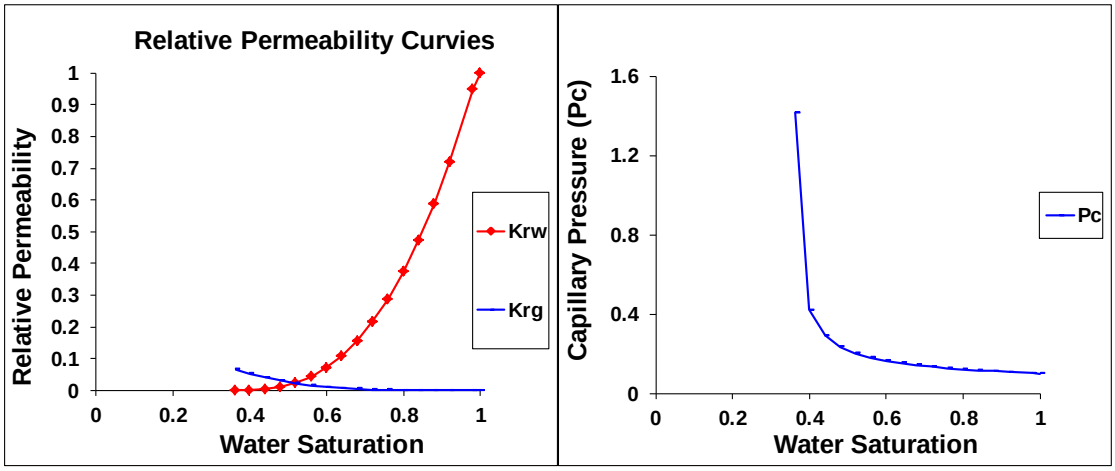

Figure 2 Relative permeability curves (left) and capillary pressure (right) used in this study (Smith et al. 2011).

The datum depth was set to be 1500 m to keep the tilted models below 800 m, in order to maintain the injected CO_2 in the supercritical phase. The models are all based on the same input data including rock compressibility, diffusion coefficients, and initial and boundary conditions are chosen in a way that ensures the different models are comparable (Table 2).

Table 1 Model Specifications, a total of 144 models were generated from all combinations of 3 types of model, 4 amplitudes, 4 tilts and 3 k_v/k_h ratios.

Model type	Amplitude (m)	Tilt (degrees)	kv/k_h
Perpendicular ridges (*perp*)	0	0	0.01
Parallel ridges (*para*)	3	1	0.1
Transition Zone (*trans*)	6	2	1
	9	5	

Table 2 Model properties.

Property			
Initial mole fraction	CO_2	H_2O	NaCl
	0.0	0.967	0.033
Water diffusion	CO_2	H_2O	

coefficients (m^2/day)	0.0001	0.0005	
Initial Pressure / Temperature	Datum Depth (m)	Datum Pressure (bar)	Temperature (C)
	1500	150	45
Rock Compressibility (1/bar)	5E-05		

It should be noted that amplitude in the *trans* models refers to the half of thickness of the transition zone.

The CO_2 injection rate was chosen to be two thirds of the CO_2 emissions of a 500 MW coal-fired power plant, which is around 2 million tons of CO_2 per year (Orr, 2009). The well was controlled by surface rate with a maximum pressure limit of 220 bars. However, in all models studied here the same amount of CO_2 was injected into the models, as the pressure did not reach the maximum bottom-hole pressure. The injector was shut after 6 years and the simulation was continued for 100 years.

The models are described by four parameters:

- type of the model: *para*, *perp* or *trans*
- amplitude (A)
- tilt (D)
- k_v/k_h ratio (K).

For instance, Model Perp-A9-D5-K001 refers to a simulation with perpendicular ridges, amplitude of 9 m, tilt of 5 degrees and k_v/k_h ratio of 0.01.

Ideally, the heterogeneity in an aquifer should be represented explicitly, so that its effect on two-phase flow can be represented, through capillary pressure effects (Saadatpoor et al. 2010). However, including such complexity in the models tested here would have led to prohibitively long simulation times. Instead, heterogeneity within the aquifer formation has been modelled using k_v/k_h, assuming that the heterogeneities are in the form of horizontal low permeability features (mudstones). We have examined 3 ratios of vertical to horizontal permeability (k_v/k_h), namely 1, 0.1 and 0.01. These could represent sandstone with negligible mudstone, one with a mudstone fraction of approximately 0.1 and one with a mudstone fraction of approximately 0.25, respectively (Ringrose et al. 2005).

3. Comparison of numerical and analytical models

Prior to investigating the effects of tilt, rugosity and k_v/k_h on CO_2 migration, a preliminary test on the numerical simulation was carried out, by comparing results with an analytical calculation. Nordbotten et al. (2005) presented an equation for the extent of plume migration in flat models (tilt equals zero) and $k_v/k_h = 1$, as follows:

$$d = \sqrt{\frac{\lambda_c Q t}{\phi \lambda_w B \pi}} \tag{2}$$

where, d refers to the length of plume, λ_c denotes for CO_2 mobility, λ_w denotes for water mobility, ϕ refers to porosity, B denotes to the reservoir thickness, Q refers to the flow rate, and t refers to time.

Taking account of the residual brine saturation, Equation (2) may be written as:

169 $$d = \sqrt{\frac{\lambda Q t}{\phi B \pi (1 - S_r)}} \quad (3)$$

170 (Okwen et al. 2010), where λ denotes the ratio of motilities of two fluids ($\frac{\lambda_c}{\lambda_w}$), and S_r is the residual
171 brine saturation. The length of the plume was calculated based on the above equation for the Perp-A0-
172 D0-K1 Model, for which the amplitude and tilt are zero and k_v/k_h ratio equals 1. Table 3 shows the
173 properties of the model that were used to calculate the length of plume (d), which equals 1207 m. This
174 validates numerical results for this case, where d = 1200 m.
175
176 Table 3 Values used to calculate length of plume in Perp-A0-D0-K1 Model

λ	Q (m^3/day)	t (day)	S_r	ϕ	B (m)	Length from Okwen (m)	Length from simulation (m)
4	6638	2190	0.364	0.2	100	1207	1200

177
178
179 **4. Plume Migration**
180 In this section the results of the effect of tilt, k_v/k_h ratio and amplitude on the plume migration are
181 presented. Later, the results of the effect of these parameters on the amount of CO_2 dissolution will be
182 discussed.
183 **4.1 Models with no Ridges or Transition Zones**
184 First, we consider models with no sinusoidal ridges (amplitude = 0) and no transition zone. Figure 3
185 shows cross-sections of the gas saturation in three models –A0-D0-K001, A0-D2-K01 and A0-D5-K1
186 – at the end of the simulation (100 years post injection). In A0-D0-K001, because the CO_2 rises
187 slowly, the gas saturation remains high in the location of the well. Also, the plume does not migrate far
188 along the underside of the caprock. On the other hand, by the end of the simulation in A0-D5-K1, all
189 the mobile CO_2 has risen to the top of the aquifer (i.e. just under the caprock) and only residual
190 saturation remains. Therefore there is more CO_2 available to migrate along the underside of the
191 caprock, aided by the high tilt. In this case, the mobile CO_2 migrates away from the injection location
192 as a narrow plume of maximum thickness 10 m. Note that in our simulations we do not observe a
193 shock in the trailing edge of the plume as predicted by Hesse et al. (2008) and MacMinn et al. (2010),
194 who both derived analytical formulae to describe plume migration using a sharp interface, vertical
195 equilibrium approximation. Further investigations of our simulations showed that, if the well is placed
196 away from the left edge (down-dip side) of the model, the CO_2 moves both down-dip and up-dip under
197 the cap rock, due to a rise in potential ($P - \rho gh$) above the injection site. In the models shown here
198 where the injector location is at the down-dip edge of the model, the highest potential was at a location
199 slightly up-dip from the injection location (due to CO_2 rising vertically), so there was still a tendency
200 for CO_2 to move down-dip, and thus spread out the trailing edge of the plume. The CO_2 distribution in
201 model A0-D2-K01 was intermediate between the two extreme models shown in Figure 3.

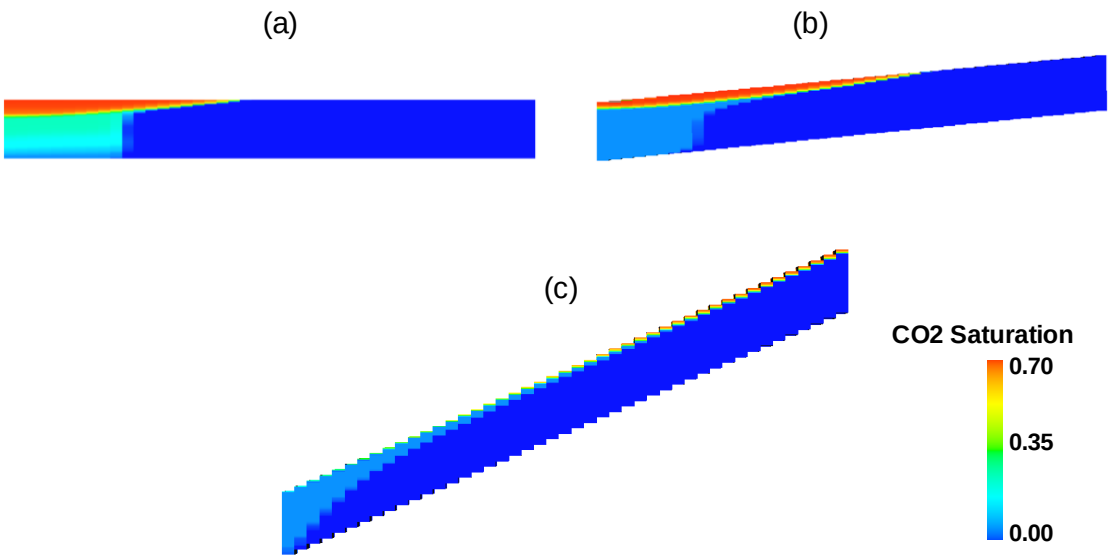

Figure 3 Cross-section of the gas saturation in three models with no sinusoidal variations on the top surfaces at 100 years post injection: a) A0-D0-K001, b) A0-D2-K01 and c) A0-D5-K1.

4.2 Sensitivity Study on the Effect of Tilt on the Plume Migration

In order to investigate the relation between the tilt and the plume migration (where CO_2 saturation is more than 10%), some additional tilted models with 3 and 4 degree tilts were constructed. Results show that the length of the plume, which is the distance where CO_2 migrates parallel to the tilt 100 years post injection, increases with tilt linearly from 0 to 4 degrees. However, after 4 degrees it increases more rapidly due to the decrease in CO_2 density (compared with the brine density) as it rises (Figure 4).

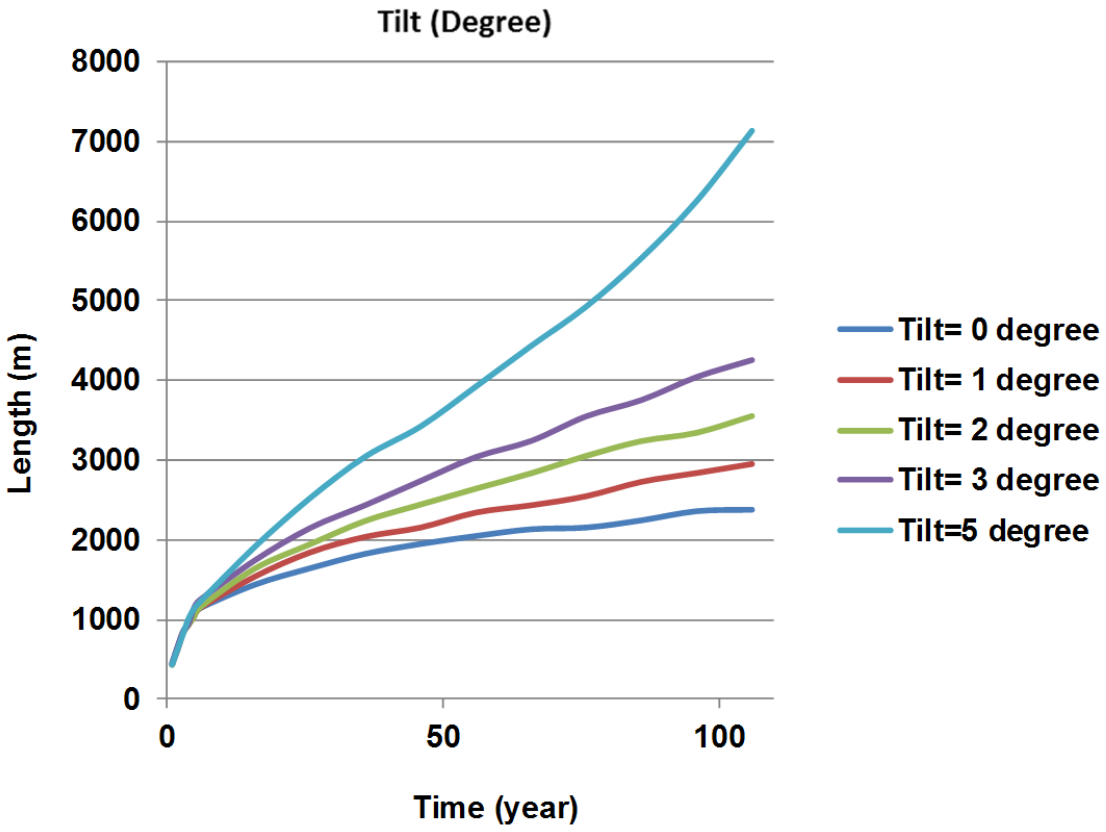

Figure 4: The length of plume at 100 years post-injection with time. The models had zero amplitude, and k_v/k_h = 1.

4.3 Plume Migration in *Para* and *Perp* Models

Figure 5 illustrates examples of plume migration in the models where the sinusoidal ridges are parallel to the tilt. As expected the ridges encourage migration up-dip. Two examples of CO_2 migration in models where the ridges are perpendicular to the dip are given in Figure 6. The perpendicular ridges hamper the migration up-dip, and lead to a broader plume. In Figure 6, the effect of k_v/k_h can also be seen: as in the cases with no sinusoidal ridges, less CO_2 reaches the top of the storage formation, and there is less plume migration.

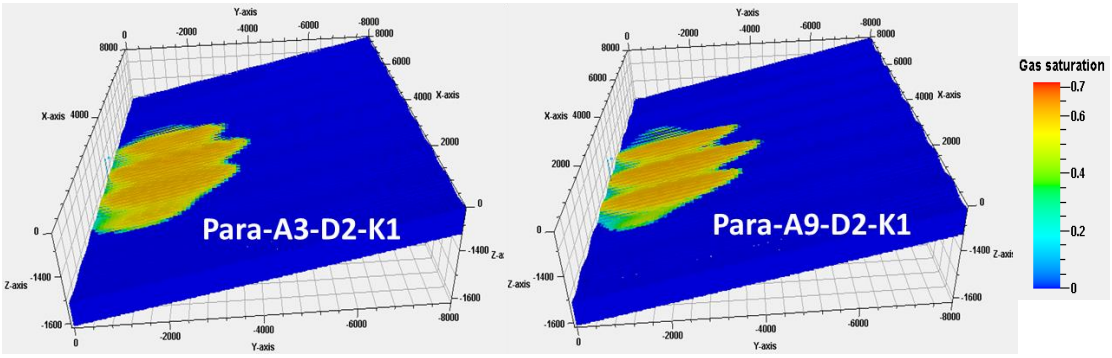

Figure 5 Gas saturation 100 years after the end of injection in two *para* models with tilt = 2° and k_v/k_h = 1. Left: amplitude = 3 m and right: amplitude = 9 m.

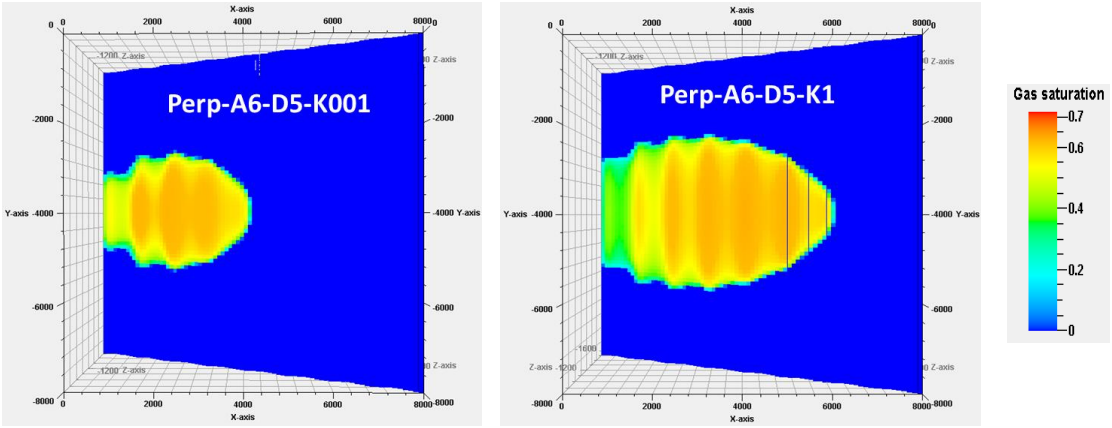

Figure 6 Gas saturation 100 years after the end of injection in two *perp* models with amplitude = 6 m, tilt = 5°. Left: k_v/k_h = 0.01 and right: k_v/k_h = 1.

A full set of results is presented in Figures 7 and 8, in the form of 3D diagrams (7a and 8a) showing the combination of all the effects: k_v/k_h, tilt and amplitude, at the end of injection and at 100 post injection, respectively. In these figures, the top box of each pair is for the *para* model and the lower one is for the *perp* models. As can be seen in Figure 7, the length of the plume at the end of injection depends very much on the k_v/k_h ratio. When k_v/k_h = 0.01, the plume rises slowly and has not reached the top of the aquifer by the end of injection. Therefore the amplitude and tilt have negligible effect. As k_v/k_h increases, the plume rises to the top of the aquifer faster and spreads out in the up-dip direction. In the k_v/k_h = 1 models, the higher the tilt the further the spread. However, note that in all these cases, the amplitude does not have a large effect because the plume has not yet had time to spread far from the injection location – the maximum distance migrated is 1400m, which is less than 1.5 times the wavelength of the sinusoidal variation. In the *para* models, though, there is a slight increase in the distance migrated at larger amplitudes due to the CO_2 being channelled along ridges.

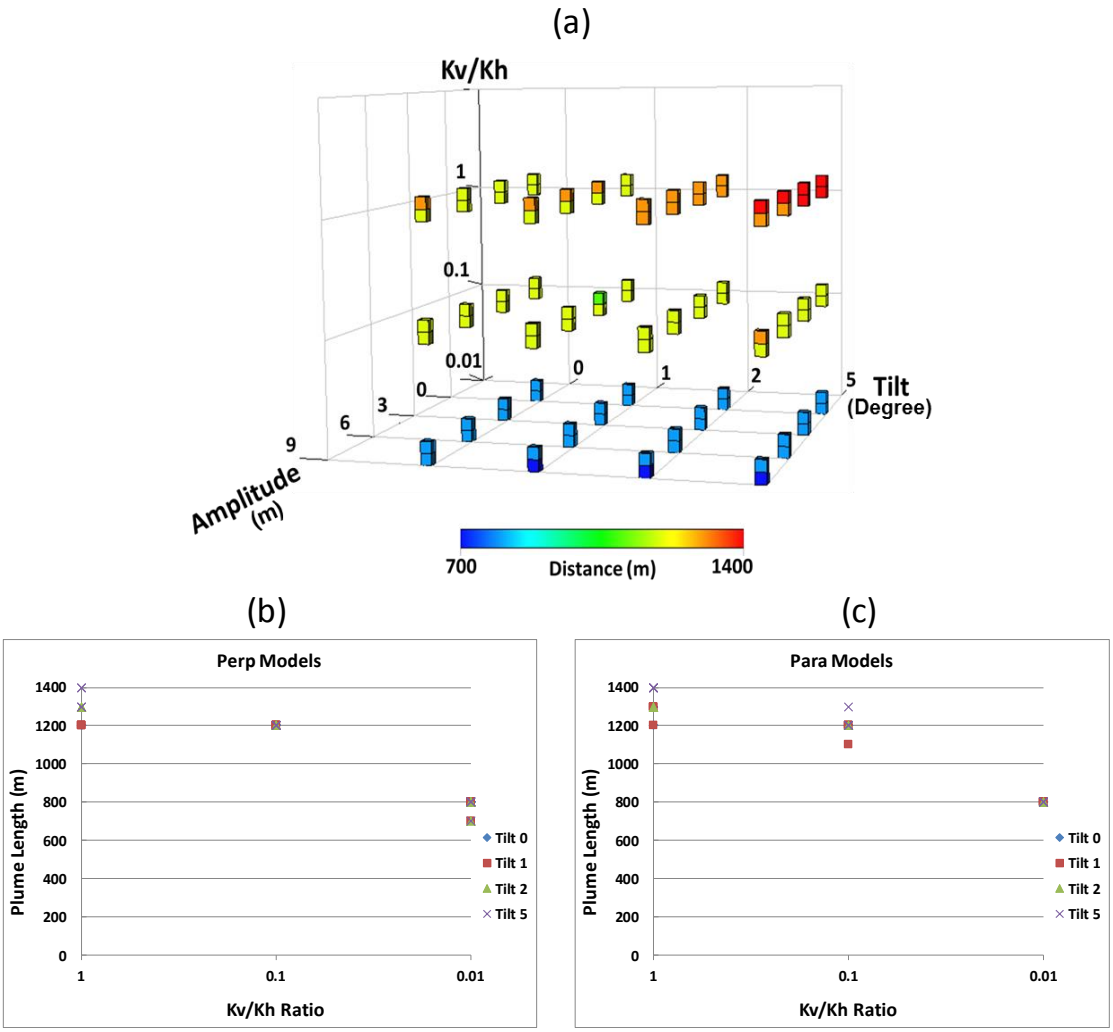

Figure 7 Length of the plume as a function of amplitude, tilt and k_v/k_h at the end of injection (a). The top box of each pair is from the *para* simulations, and the bottom box from the *perp* simulations. The length of the plume vs k_v/k_h ratio at the end of injection period in the *perp* models (b) and *para* models (c).

Figure 8 shows the length of the plume measured under the caprock, at the end of the simulations (100 years post-injection). The dominant effect is the tilt which increases the length of the plume in both the *para* and *perp* models. The k_v/k_h ratio has the second most significant effect. This is especially noticeable in the case with tilt = 5°. As mentioned above, in cases with low k_v/k_h (0.01), the CO_2 takes a long time to rise to the top of the aquifer, and therefore there is less CO_2 available to migrate outward away from the injection point. The amplitude does not have a significant effect when considering the *para* and *perp* models separately. However, there is noticeable difference in the length of the plume between the models: the migration is greater in the *para* models, as expected. In the *perp* models, one might expect the amplitude to have a significant effect in trapping the CO_2, since Figure 3 shows that, in the models with A = 0, the plume becomes thinner and spreads further as the tilt increases. However, as the tilt increases, the volume which can be trapped under a crest decreases, allowing the CO_2 to migrate further. (See discussion below.)

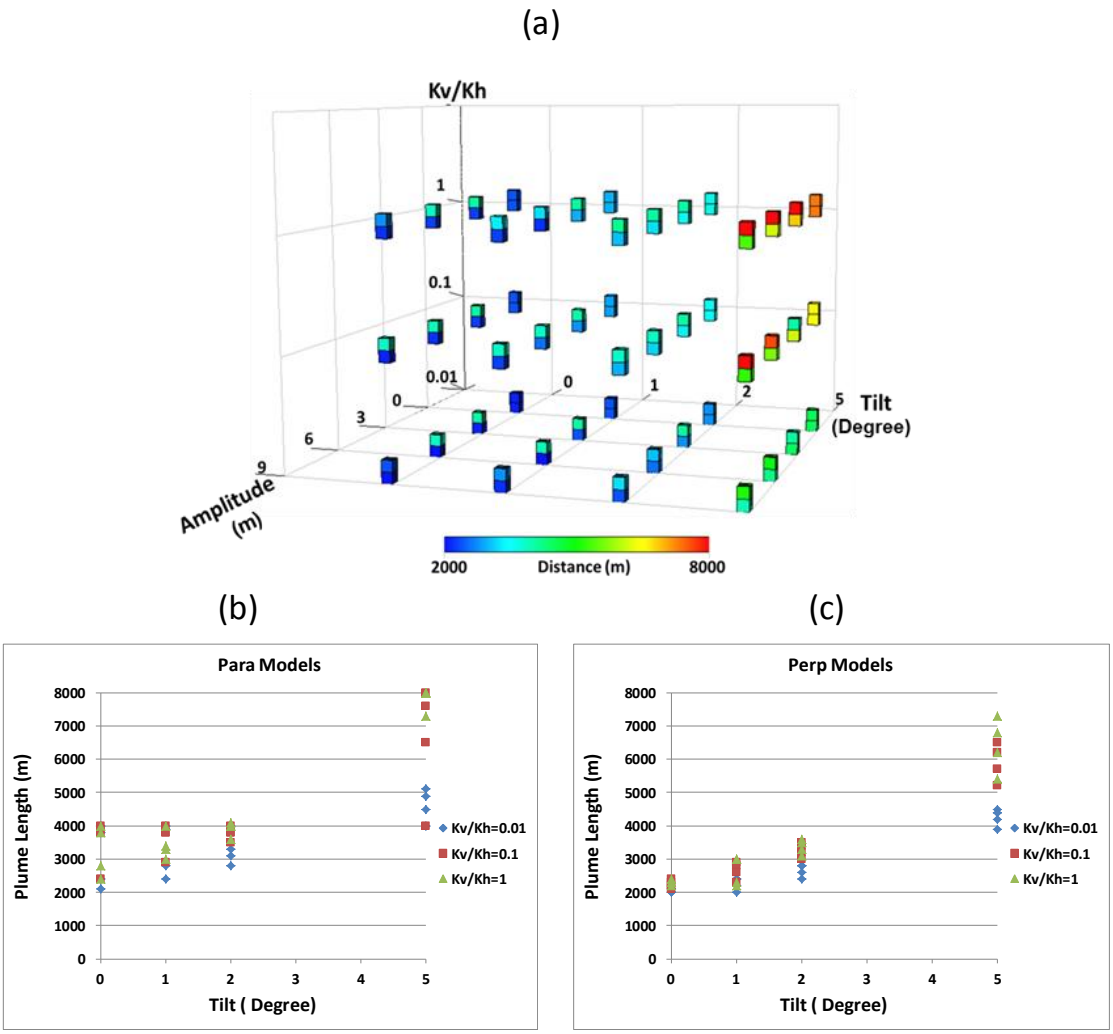

Figure 8 Length of the plume as a function of amplitude, tilt and k_v/k_h at 100 years post injection (a). The top box of each pair is from the *para* simulations, and the bottom box from the *perp* simulations. Note that the colour scale is different from that in Figure 7. The length of the plume vs tilt in the *para* models (b) and *perp* models (c).

4.4 Migration in the *trans* models

In the *trans* models, the presence of the discontinuous shale (or mudstone) layers hampered the rise of the CO_2 in the transition zone, and the resulting CO_2 distribution at the top of the aquifer was patchy. The distribution of CO_2 obviously depends on the realisation of the stochastic shales. Only, one realisation of each model for amplitudes of 3, 6 and 9 m (thickness of transition zone = 6, 12 and 18 m) was generated. Some qualitative conclusions may be drawn from these simulations. The analysis of these results focused on the migration of CO_2 at the end of the simulation (100 years post injection). Figure 9 demonstrates the effect of k_v/k_h, tilt and amplitude on the length of plume measured under the caprock in *trans* models at 100 years post injection. Figure 10 shows an example of the gas saturation in 3 *trans* models. As with the *para* and *perp* models, the tilt has the main effect at 100 years post injection: as tilt increases, the maximum distance migrated at the top of the aquifer increases. The maximum distance migrated under the caprock in the *trans* models, is less than in the *para* models, but comparable to the *perp* models. When the angle of tilt is zero, the CO_2 may reach the top of the aquifer

in any direction from the well (case not shown). As the angle of tilt increases, the CO_2 is more likely to reach the top of the aquifer in the up-dip direction. The k_v/k_h ratio had some effect – as k_v/k_h increased, the maximum distance migrated increased. The effect of amplitude (thickness of transition zone) on the plume migration at the very top of the models is as expected: the furthest plume migration is observed in the models with amplitude zero (no shale layers) compared to other models. This is due to the fact that there was no interbeded shale layer to hamper the CO_2 migration vertically. The volume of CO_2 reaching the top of the aquifer decreased in models with amplitudes 3, 6 and 9 m. However, there wasn't any particular trend between plume migration in models with amplitudes of 3, 6 and 9 m. This demonstrates the unpredictability of the migration of CO_2 in aquifers where there is a transition zone.

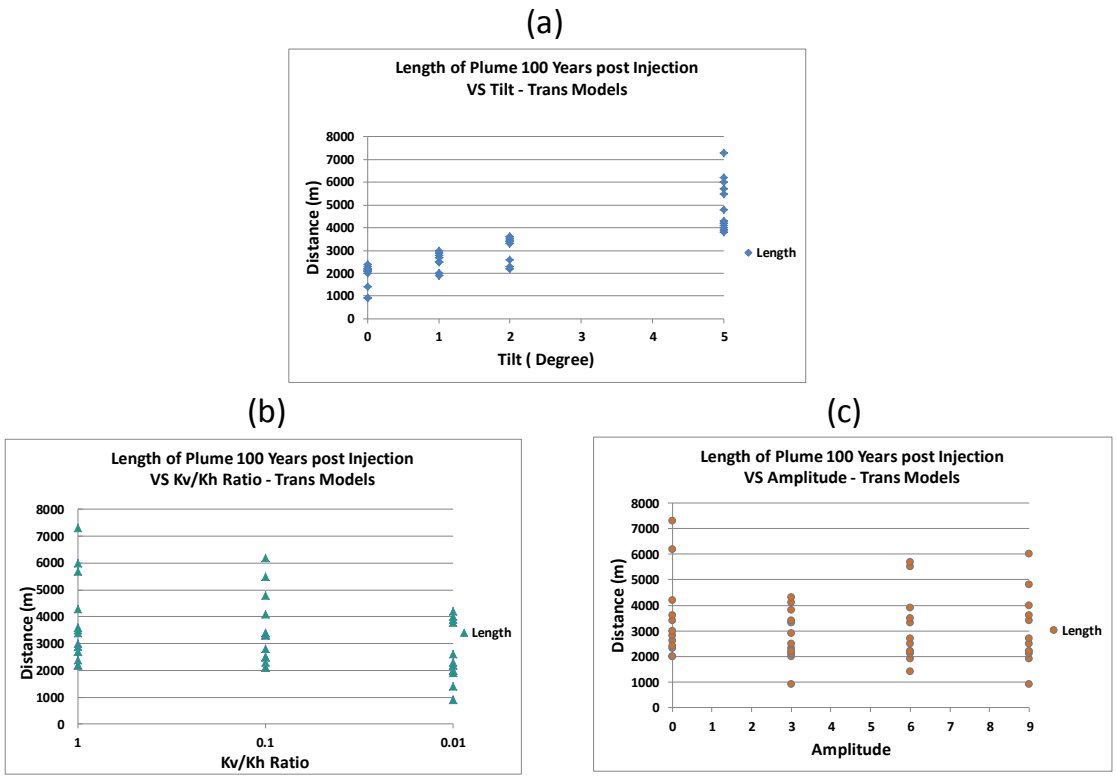

Figure 9 Length of the plume as a function of tilt (a), k_v/k_h ratio (b) and amplitude (c) in *trans* models at 100 years post injection.

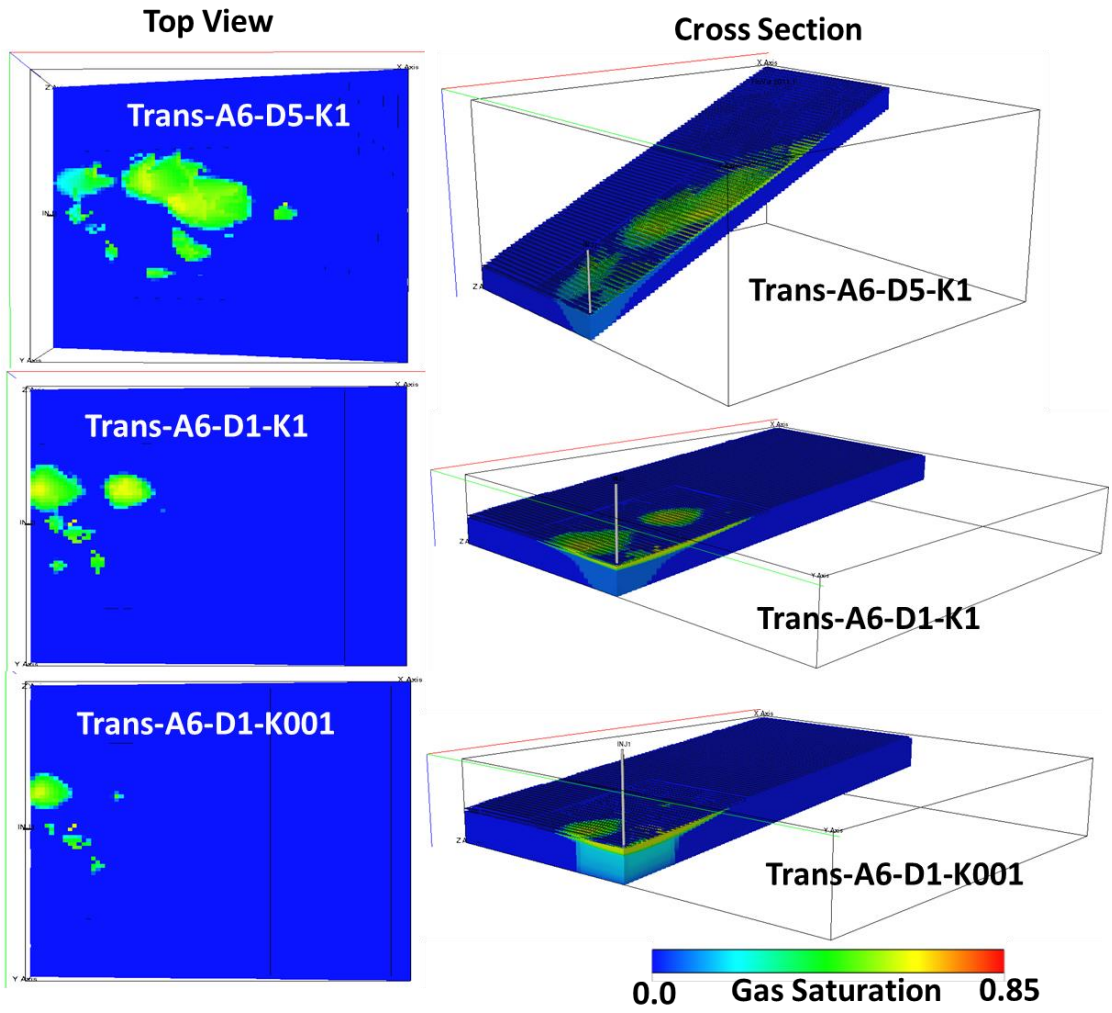

Figure 10 The CO_2 distribution at the top of the aquifer in 3 *trans* models –A6-D5-K1, A6-D1-K1 and A6-D1-K001, at 100 years after the end of injection.

5. Dissolution

It is of interest to examine the amount of dissolution which arises in the different models. Figure 11 shows the amount of dissolution at the end of injection. This figure includes results for the *para*, *perp* and *trans* models. The results show that dissolution is completely dominated by the k_v/k_h ratio. The lower k_v/k_h, the further the plume spreads out laterally, and therefore contacts more brine. Figure 12 illustrates the amount of dissolution at the end of the 100-year post-injection period (Note again the difference in colour scales between the figures at the end of injection and the end of the simulation.). This time (as with the migration distance), the tilt has the most significant effect in all of the models – *para*, *perp* and *trans*. At this stage, the amount of tilt aids migration of the CO_2, and so increases the amount of contact of CO_2 with fresh brine. In the high tilt models, with $k_v/k_h \geq 0.1$, the amount of dissolution tends to be greatest in the *trans* models and least in the *perp* models. In the *trans* models, this is due to the plume being dispersed by the shales near the top of the aquifer, so the CO_2 comes into contact with more brine. On the other hand, in the *perp* models, there is CO_2 trapping in the crests, so the CO_2 contacts less brine.

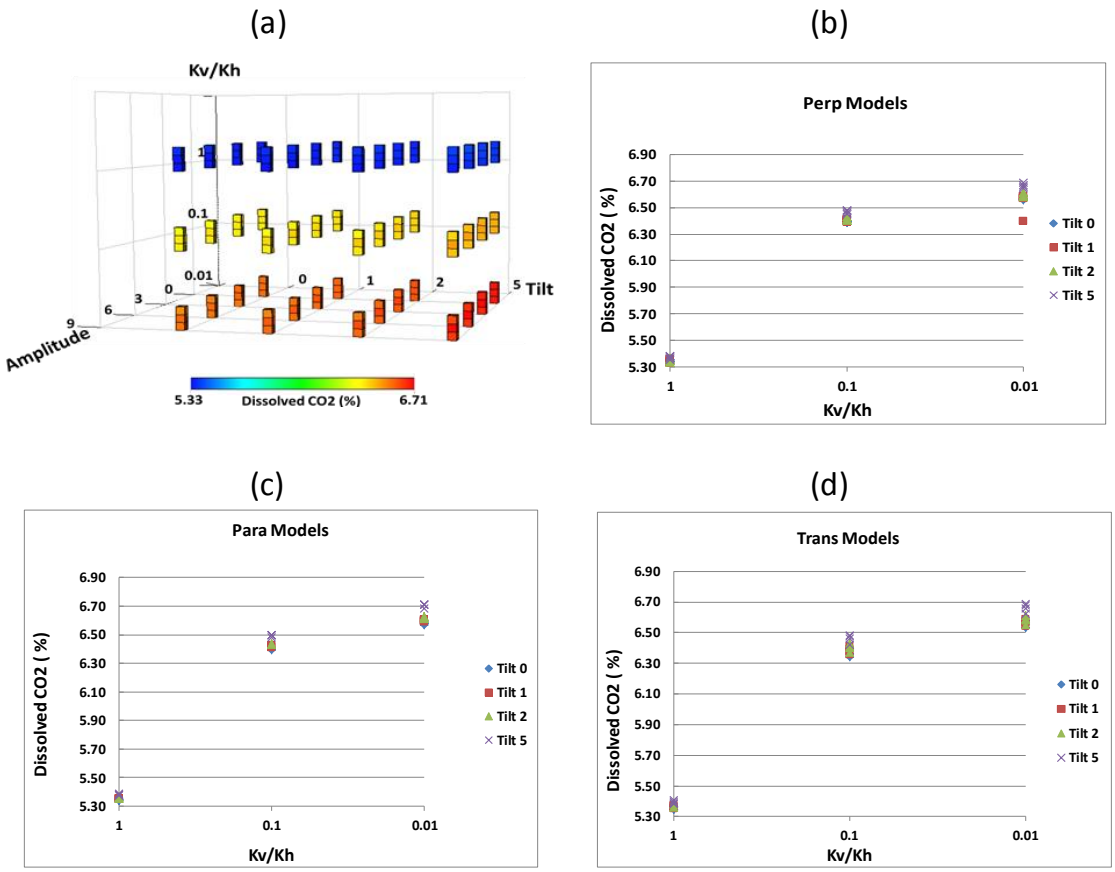

Figure 11 Dissolved CO_2 at the end of injection for the *trans*, *para* and *perp* models (a, b, c and d). The top box at each point refers to the *trans* models, the middle one refers to the *para* models and the bottom one refers to the *perp* models (a). The amount of dissolved CO_2 in percentage at the end of injection vs k_v/k_h ratio in the *perp* models (b), *para* models (c) and *trans* models (d).

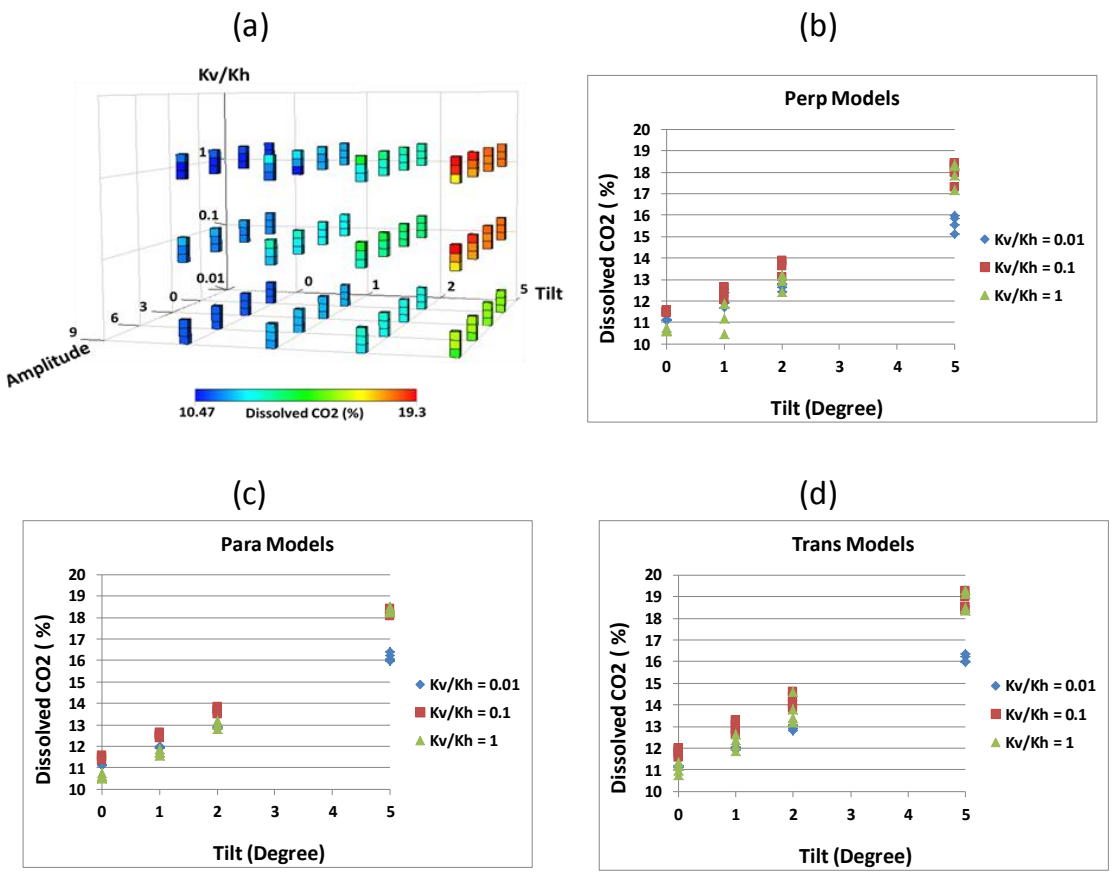

Figure 12 Dissolved CO_2 100 years post injection period for *trans*, *para* and *perp* models (a, b, c and d). The top box at each point refers to the *trans* models, the middle one refers to the *para* models and the bottom one refers to the *perp* models (a). The amount of dissolved CO_2 as a percentage 100 years post injection vs tilt in the *perp* models (b), *para* models (c) and *trans* models (d).

6. Analytical Calculations of trapping

In this section an equation for the relationship between tilt (θ), amplitude (A), and wavelength (λ) is presented that can be deployed to find out under what conditions the morphology of top surface could make a significant difference, and what will never have an effect. In the *perp* models, the effects of small scale amplitudes on the plume migration and CO_2 dissolution are diminished when the tilt increases. This is due to the fact that less CO_2 will trap locally under ridges. For instance in sine-wave models, the amount of CO_2 that can be trapped under each wavelength is decreased by approximately 2/3 as the tilt is increased from 0 to 1 (see the calculations in Appendix A). The area under a non-tilted sine-wave model is equal to $A\lambda/\pi$. It can be concluded that as long as $\tan(\theta) < (2\pi A/\lambda)$ a percentage of CO_2 will be trapped under ridges. Therefore, this could be a simple important measurement tool to identify whether the topography of top surface has an important role in CO_2 trapping or not.

Figure 13 shows the effect of increasing the tilt in models with different amplitudes, and Table 4 indicates which models of those studied (A = 3 m – 9 m and D = 0° – 5°) will give rise to trapping and which will not.

Results show that for models with tilt of more than 1 degree, and amplitude less than 3 metres, morphology cannot make a significant effect on the CO_2 trapping.

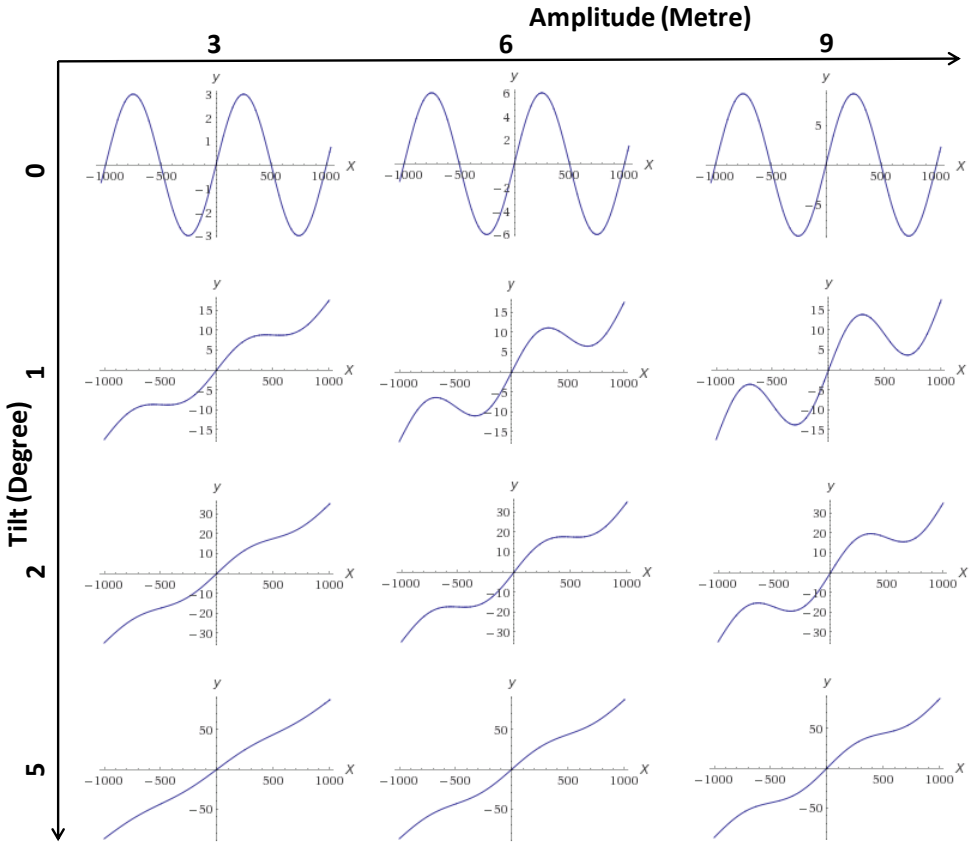

Figure 13 Relationship between tilt and amplitude when the wavelength equals 1000 metres over a distance of 2λ. By increasing the tilt, the top morphology gets closer to a tilted flat surface where no CO_2 will be trapped.

Table 4 Relationship between tilt (θ) and amplitude (A) and trapping (T = trapping and NT = no trapping).

Amplitude (m) / Tilt (Degree)	3	6	9
0	T	T	T
1	T	T	T
2	NT	T	T
5	NT	NT	NT

7. Concluding Remarks

In this study, we investigated CO_2 plume migration in a range of aquifer models. The focus was mainly on the interface between the aquifer and the caprock, and we tested the effect of rugosity and tilt at the interface, and the presence of a transition zone between the aquifer and caprock, in the form of stochastically distributed shales. We also explored the influence of the k_v/k_h ratio in the aquifer.

Results showed that the most influential factor during injection was the k_v/k_h ratio, which determines the length of time which the CO_2 takes to reach the top of the aquifer. Aquifer heterogeneity is important, and when present should be included in estimations of CO_2 migration. Not only does the effective vertical permeability have a significant effect during injection, but it also influences the distance migrated at later times.

In the post-injection period, the tilt was most influential. The amplitude of the sinusoidal variation had some effect. In the *para* models, it increased the migration distance, while in the *perp* models, it hindered migration. However, trapping was limited in the tilted models, and we derived a simple equation to estimate the maximum tilt for trapping as a function of amplitude and wavelength of the sinusoidal fluctuation at the interface.

The possibility of a transition zone between the aquifer and caprock has been largely overlooked in previous studies, although this has been observed in outcrop (Shariatipour et al. 2012, 2014; Newell and Shariatipour 2016). The presence of a transition zone is beneficial, as CO_2 may be trapped under shales near the top of the aquifer, limiting the amount of CO_2 reaching the caprock. In addition, the amount of dissolution is enhanced in *trans* models, due to the shales dispersing the CO_2 plume which therefore contacts more brine. At the Sleipner storage cite, the CO_2 plume migration beneath the caprock (top seal) has been studied extensively and CO_2 plume behaviour calibrated against monitoring data using numerical simulation results and seismic data (Cavanagh 2013; Cavanagh and Haszeldine 2014; Chadwick et al., 2004, 2006; Chadwick and Noy, 2010; Singh et al., 2010; Nilsen et al., 2011; Bandilla et al., 2014). Currently, none of the conventional simulations methods (full physics, or vertical equilibrium) is capable of reproducing the observed plume (Cavanagh 2013; Bandilla et al., 2014). Our results show that small-scale features just beneath the caprock (surface rugosity, heterogeneity and k_v/k_h ratio), which will not be identified by seismic data, could have an effect on plume migration at the top of the storage formation. Thus, considering such effects in a real case scenario such as Sleipner could help further in the prediction of CO_2 plume behaviour beneath the caprock.

In general, the results of this work demonstrate that reservoir characterisation of potential CO_2 storage sites is very important, in order to assess CO_2 migration and to predict the location of boundaries for the storage complex. This includes assessment of heterogeneities within the aquifer itself, and the nature of the aquifer/caprock interface.

Acknowledgements

This work was funded by the Scottish Carbon Capture and Storage Consortium (SCCS) and Computer Modelling Group Foundation (CMG). This financial support is gratefully acknowledged. Authors thank Schlumberger for the use of ECLIPSE 300 and Petrel and Amarile for the use of the RE-Studio.

References

BANDILLA, K.W., CELIA, M.A. AND LEISTER. E., 2014, Impact of model complexity on CO_2 plume modelling at Sleipner. *Energy Procedia*, 63, 3405–3415.

CAVANAGH, A., 2013. Benchmark calibration and prediction of the Sleipner CO_2 plume from 2006 to 2012. *Energy Procedia*, 37, 3529-3545.

CAVANAGH, A. J., AND HASZELDINE. R. S., 2014, The Sleipner storage site: Capillary flow modeling of a layered CO_2 plume requires fractured shale barriers within the Utsira Formation, *International Journal of Greenhouse Gas Control*, 21, 101–112.

CHADWICK, R. A., ZWEIGEL. R. A., GREGERSEN. P.,U., KIRBY. G. A., HOLLOWAY. S., AND JOHANNESSEN. P.N., 2004. Geological reservoir characterization of a CO_2 storage site: The Utsira Sand, Sleipner, northern North Sea, Energy, 29, 1371–1381.

CHADWICK, A., R. ARTS, O. EIKEN, P. WILLIAMSON, AND G. WILLIAMS., 2006. Geophysical monitoring of the CO_2 plume at Sleipner, North Sea, in Advances in the Geological Storage of Carbon Dioxide, pp. 303–314, Springer, Dordrecht, Netherlands.

CHADWICK, R.A., NOY, D., ARTS, R. & EIKEN, O., 2009. Latest time-lapse seismic data from Sleipner yield new insights into CO_2 plume development, Energy Procedia, 1, 2103-2110.

CHADWICK, R. A., & NOY, D. J., 2010. History-matching flow simulations and time-lapse seismic data from the Sleipner CO_2 plume. In *Geological Society*, London, Petroleum Geology Conference series (Vol. 7, pp. 1171-1182). Geological Society of London.

JENKINS, C., CHADWICK, A., & HOVORKA, S. D., 2015. The state of the art in monitoring and verification-ten years on. *International Journal of Greenhouse Gas Control*, 40, 312-349.

GASDA, S.E., NORDBOTTEN, J.M. & CELIA, M.A., 2009. Vertical equilibrium with sub-scale analytical methods for geological CO_2 sequestration, Computational Geosciences, 13, 469-481.

GASDA, S. E., NILSEN, H. M., DAHLE, H. K., & GRAY, W. G. 2012. Effective models for CO_2 migration in geological systems with varying topography. *Water Resources Research*, 48, p. W10546.

GOATER, A., BIJELJIC, B., AND BLUNT, M. J., 2013. Dipping open aquifers—The effect of top-surface topography and heterogeneity on CO_2 storage efficiency. *International Journal of Greenhouse Gas Control*, 17**,** 318-331.

HESSE, M. A. (2008). *MATHEMATICAL MODELING AND MULTISCALE SIMULATION OF C0₂ STORAGE IN SALINE AQUIFERS* (Doctoral dissertation, Stanford University).

MacMINN, C.W., SZULCZEWSKI, M.L. and JUANES, R., 2010. "CO_2 migration in saline aquifers. Part 1. Capillary trapping under slope and groundwater flow", J. *Fluid Mech*., 662, 329-351.

NILSEN, H., P. A. HERRERA, M. ASHRAF, I. LIGAARDEN, M. IDING, C. HERMANRUD, K. LIE, J. M. NORDBOTTEN, H. K. DAHLE, AND E. KEILEGAVLEN 2011, Field-case simulation of CO_2-plume migration using vertical-equilibrium models, Energy Procedia, 4, 3801–3808.

NILSEN, H. M., SYVERSVEEN, A. R., LIE, K.-A., TVERANGER, J. & NORDBOTTEN, J. M., 2012. Impact of top-surface morphology on CO_2 storage capacity. *International Journal of Greenhouse Gas Control*, 11**,** 221-235.

NEWELL A.J., & SHARIATIPOUR S.M., 2016. Linking outcrop analogue with flow simulation to reduce uncertainty in sub-surface carbon capture and storage: an example from the Sherwood Sandstone Group of the Wessex Basin, UK. Geological Society, London, Special Publications, 436. http://doi.org/10.1144/SP436.2.

NORDBOTTEN, J. M., CELIA, M. A., & BACHU, S., 2005. Injection and storage of CO_2 in deep saline aquifers: Analytical solution for CO_2 plume evolution during injection. Transport in Porous media, 58(3), 339-360.

OKWEN, R. T., STEWART, M. T., & CUNNINGHAM, J. A., 2010. Analytical solution for estimating storage efficiency of geologic sequestration of CO_2. International Journal of Greenhouse Gas Control, 4(1), 102-107.

ORR, F. M. (2009). Onshore geologic storage of CO_2. *Science*, *325*(5948), 1656-1658.

PEARCE, J.M., HANNIS, S.J., KIRBY, G.A., DELPRAT-JANNAUD, M.C., AKHURST, M.C., NIELSEN, C., FRYKMAN, P. & DLAHOFF, F., 2013. How to submit a CO_2 storage permit: Identifying appropriate geological site characterization to meet European regulatory requirements. Energy Procedia, 37, 7783-7792.

RINGROSE, P., NORDAHL, K. & WEN, R., 2005. Vertical permeability estimation in heterolithic tidal deltaic sandstones, Petroleum Geoscience, 11, 29-36.

SAADATPOOR, E., BRYANT, S.L. & SEPEHRNOORI, K., 2010. New trapping mechanism in carbon sequestration, Transport in Porous Media, 82, 3 – 17.

SCHLUMBERGER, 2013. Eclipse Technical Manual

SHARIATIPOUR, S.M., PICKUP, G.E., STOW, D.A.V., AND MACKAY, E.J. 2012. The Effects of Aquifer/Caprock Interface on CO_2 Storage Capacity and Security. 3rd EAGE CO_2 Geological Storage Workshop.

SHARIATIPOUR, S.M., PICKUP, G.E., MACKAY, E.J., 2016. Investigation of CO_2 Storage in a Saline Formation with an Angular Unconformity at the Caprock Interface. Petroleum Geoscience, *22*(2), 203-210.

SHARIATIPOUR, S. M., PICKUP, G. E., & MACKAY, E. J. 2014. The Effect of Aquifer/Caprock Interface on Geological Storage of CO_2. Energy Procedia, 63, 5544-5555.

SINGH, V., A. CAVANAGH, H. HANSEN, B. NAZARIAN, M. IDING, AND P. RINGROSE 2010, Reservoir modeling of CO_2 plume behavior calibrated against monitoring data from Sleipner, Norway, paper SPE 134891 presented at the SPE Annual Technical Conference and Exhibition, Society of Petroleum Engineers, Soc. of Petrol. Eng., Florence, 19-22 Sept.

SMITH, M., CAMPBELL, D., MACKAY, E. and POLSON, D., 2011. CO_2 Aquifer Storage Site Evaluation and Monitoring: Understanding the Challenges of CO_2 Storage: Results of the CASSEM Project. Scottish Carbon Capture and Storage. Available from http://www.sccs.org.uk/expertise/reports.

SPYCHER, N. and PREUSS, P., 2005. CO_2-H_2O mixtures in the geological sequestration of CO_2. II. Partitioning in chloride brines at 12-100 C and up to 600 bar, Geochimica et Cosmochimica Acta, 69 (13), 3309-3320.

WILLIAMS, J.D.O., JIN, M., BENTHAM, M., PICKUP, G.E., HANNIS, S.D. & MACKAY, E.J., 2013. Modelling carbon dioxide storage within closed structures in the UK Bunter Sandstone Formation, International Journal of Greenhouse Gas Control, 18, 38-50.

ZHU, C., ZHANG, G., LU, P., MENG, L., & JI, X., 2015. Benchmark modeling of the Sleipner CO_2 plume: Calibration to seismic data for the uppermost layer and model sensitivity analysis. International Journal of Greenhouse Gas Control.in Press.

Appendix A

Simple Analytical Calculations of trapping

Using Equation (1) and tilt $\theta = 0$, the area under a non-tilted sine wave model (A1 in Figure A.1) can be calculated.

$$Z = Z_0 + A(Sin(\frac{2\pi x}{\lambda})) + x(\tan\theta)$$

where λ is wavelength.

Substituting $\theta = 0$,

$$Z = Z_0 + A(Sin(\frac{2\pi x}{\lambda})) \quad \text{(A.1)}$$

Assuming $Z_0 = 0$, and integrating over one wavelength:

$$Area = \int A(sin(\frac{2\pi x}{\lambda}))dx = A\lambda$$

As shown in Figure A.1, at a certain tilt, the amount of trapping will be approximately equal to the area under the top half of a sine wave, i.e. the integral under the sine wave between angles of 0 and π. The resulting area is equal to $A\lambda/\pi$, which is approximately equal to $A\lambda/3$. This occurs when the average height of the sine wave increases by approximately one amplitude over a distance of $\lambda/2$. In other words $\theta = \tan^{-1}(9/500) = 1^o$.

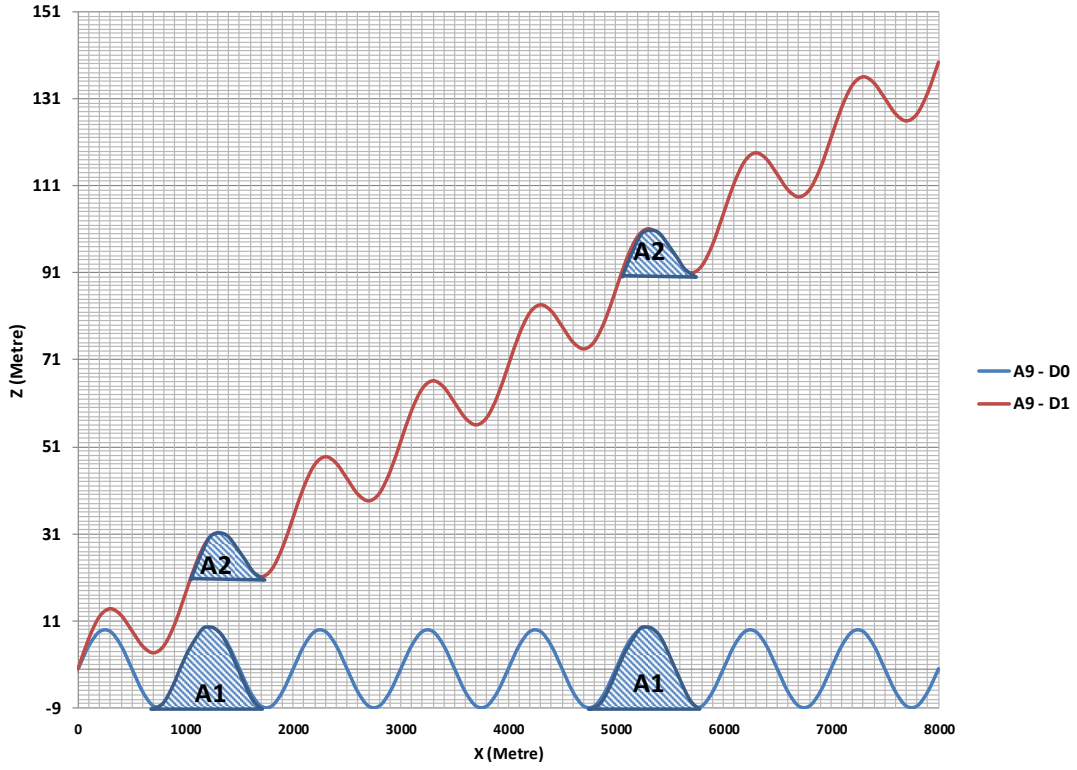

Figure A.1 Decrease in local structural trapping due to increase in tilt angle. A1 shows the area under a

wavelength in a flat *perp* model with amplitude of 9 metres and A2 shows the area under a wavelength in a 1 degree tilted *perp* model, also with amplitude of 9 metres.

The tilt at which the amount of trapping falls to zero can be calculated as follows:

Differentiating Equation (1),

$$\frac{dz}{dx} = \tan(\theta) + \frac{2\pi A}{\lambda}\cos(\frac{2\pi x}{\lambda}) \qquad \text{(A.2)}$$

For trapping, this must be always negative for some value of *x*. But, for no trapping, this must always be non-negative $(dz/dx \geq 0)$. The minimum of a cosine is -1, so the minimum gradient is

$$\frac{dz}{dx} = \tan(\theta) - \frac{2\pi A}{\lambda} \geq 0$$

Thus;

$$\tan(\theta) \geq \frac{2\pi A}{\lambda} \qquad \text{(A.3)}$$

If the minimum gradient is zero, then

$$\tan(\theta) = \frac{2\pi A}{\lambda}$$

Therefore θ is given by:

$$\theta = \tan^{-1}(\frac{2\pi A}{\lambda}). \qquad \text{(A.4)}$$